

Large dynamic scissoring mode displacements coupled to band gap opening in Hybrid Perovskites

Tobias A. Bird,¹ Jungshen Chen,² Manila Songvilay,³ Chris Stock,⁴
Michael T. Wharmby,⁵ Nicholas C. Bristowe,⁶ and Mark S. Senn^{1,*}

¹*Department of Chemistry, University of Warwick,
Gibbet Hill, Coventry, CV4 7AL, United Kingdom*

²*Nano-Science Center & Department of Chemistry,
University of Copenhagen, Universitetsparken 5, 2100 Copenhagen, Denmark*

³*Institut Néel, CNRS and Université Grenoble Alpes, 38000 Grenoble, France*

⁴*School of Physics and Astronomy, University of Edinburgh, Edinburgh EH9 3FD, United Kingdom*

⁵*Deutsches Elektronen-Synchrotron (DESY), Notkestr. 85, 22607 Hamburg, Germany*

⁶*Centre for Materials Physics, Durham University,
South Road, Durham DH1 3LE, United Kingdom*

(Dated: August 13, 2021)

Hybrid perovskites are a rapidly growing research area, having reached photovoltaic power conversion efficiencies of over 25 %. We apply a symmetry-motivated analysis method to analyse X-ray pair distribution function data of the cubic phases of the hybrid perovskites MAPbX_3 ($X = \text{I, Br, Cl}$). We demonstrate that the local structure of the inorganic components of MAPbX_3 ($X = \text{I, Br, Cl}$) are dominated by scissoring type deformations of the PbX_6 octahedra. We find these modes to have a larger amplitude than equivalent distortions in the A-site deficient perovskite ScF_3 and demonstrate that they show a significant departure from the harmonic approximation. Calculations performed on an all-inorganic analogue to the hybrid perovskite, FrPbBr_3 , show that the large amplitudes of the scissoring modes are coupled to an opening of the electronic band gap. Finally, we use density functional theory calculations to show that the organic MA cations reorientate to accommodate the large amplitude scissoring modes.

I. INTRODUCTION

Molecular perovskites, also known as hybrid perovskites, are a fast growing research area in photovoltaics, due to their low cost to make and rapid increase in efficiency (from 3.9 % in 2009¹ to > 25 % today²⁻⁴). These materials have the general structure and chemical formula of traditional perovskites (ABX_3), but where they differ is that the A site cation is organic. The most frequently studied of this class of materials are the methylammonium (MA) lead halides, which have the general formula $\text{CH}_3\text{NH}_3\text{PbX}_3$ ($X = \text{I, Br, Cl}$), commonly abbreviated to MAPbX_3 . In addition to their high conversion efficiency, this class of hybrid perovskites have other desirable photovoltaic properties, such as long charge carrier lifetimes⁵, mobility⁶ and diffusion lengths⁷, a high absorption coefficient⁸, and a direct band gap¹. These properties couple together to create a device that has a high density of charge carriers with a strong barrier against recombination, all whilst needing much less material than traditional solar cell materials, and without the need for a high energy input manufacturing process⁹.

Whilst perovskite oxides are a well studied class of materials due to the wide range of desirable properties exhibited by them, less is understood about the structure-property relationship in halide perovskites, particularly the hybrid perovskite family. Having a methylammonium ion rather than a metal ion at the A site results in the A site possessing an electric dipole moment rather than a point charge, so the dynamics of these ions are the focus of a lot of research in these hybrid

perovskites. In the higher temperature tetragonal and cubic phases, the alignment of the ions appears to be disordered¹⁰⁻¹³, however they could form small domains below the length scale required for coherent diffraction where the molecules are aligned. The dynamics of their rotations, and any local order, could have a large contribution to the properties of the material. For example, the interaction between phonons and the rotational degrees of freedom of the MA cations has been shown to have an impact on thermal conductivity¹⁴. The changes in dynamics are thought to be closely linked to the structural changes of the material with temperature, and it is still unknown how the dynamics affect the properties of this material as a photovoltaic. Another question that has still not been fully solved is whether the configuration of the MA cations lead to this class of materials being ferroelectric^{10,15-17}.

Use of X-ray single crystal and powder diffraction has led to a good understanding of the different structural phases of these materials. Similarly to a large number of perovskites, all of the single-halide MAPbX_3 materials have cubic symmetry at high temperatures and undergo symmetry-lowering phase transitions to tetragonal and orthorhombic structures at lower temperatures¹⁸. Most experimental studies agree that there are 3 structural phases for MAPbI_3 and MAPbCl_3 , however there is a 4th phase for MAPbBr_3 which is preferred for a small temperature range (*ca.* 150-155 K), commonly thought to be an incommensurate phase¹⁹. In the cubic phase, the MA cation is thought to be fully disordered, with recent advances made using techniques such as NMR and

quasi-elastic neutron scattering showing that the MA cation is close to having the orientational freedom of a free MA cation^{20,21}. As the inorganic framework undergoes structural phase transitions, lowering the average symmetry from cubic $Pm\bar{3}m$, the orientational freedom of the MA cation is restricted, becoming fully ordered in the orthorhombic phases^{12,22}. This shows that the organic molecular and inorganic framework dynamics in $MAPbX_3$ are inherently linked^{23,24}. In addition to experimental studies, computational methods have seen a lot of use in this, and other, areas of research in hybrid perovskites²⁵⁻²⁹. Both classical molecular dynamics and DFT simulations have demonstrated a link between the different phases of $MAPbI_3$ and the preferred orientations of the MA cations³⁰. Work from Quarti *et al* has demonstrated that the configuration of the MA cations has a significant effect on the properties of the material, such as its electronic band structure^{31,32}. This underlines why it is important to fully understand the structure-property relationship in these materials. Despite the knowledge that the organic molecular and inorganic framework dynamics are linked *via* hydrogen bonding interactions, it is currently unclear how this interaction affects the dynamics as a whole.

The bands forming the top of the valence bands and the bottom of the conduction band in the electronic structure of the methylammonium lead halides will be dominated by Pb and X ($X = I, Br, Cl$) electrons^{24,33}. Therefore, regardless of the role of the MA cation in stabilising particular distortions, it is necessary to establish good models for the dynamic distortions in the PbX_3 framework. In this work, we aim to probe the dynamics of the inorganic framework of the cubic phases of the three single-halide $MAPbX_3$ materials. We have recently demonstrated how by using a symmetry motivated approach to analysing PDF data we can gain extra information on disorder and dynamics within a system. Our study on $BaTiO_3$ has shown that this method is very sensitive to primary order parameters and is a powerful tool to analyse order-disorder phase transitions³⁴. Both this study and our more recent work on the negative thermal expansion materials SeF_3 and $CaZrF_6$ has demonstrated that this method is also sensitive to soft phonon modes and has also revealed substantial deviations from the crystallographic average structure in these materials³⁵. Here, we use X-ray total scattering data, which is much more sensitive to the inorganic framework than the molecular cations, to probe the characters of the low lying excitations of the cubic phases of the methylammonium lead halides.

II. EXPERIMENTAL DETAILS AND DATA ANALYSIS

$MAPbI_3$ was prepared using the inverse temperature crystallisation method³⁶. Briefly, equal molar amounts of MAI and PbI_2 were dissolved in a solvent

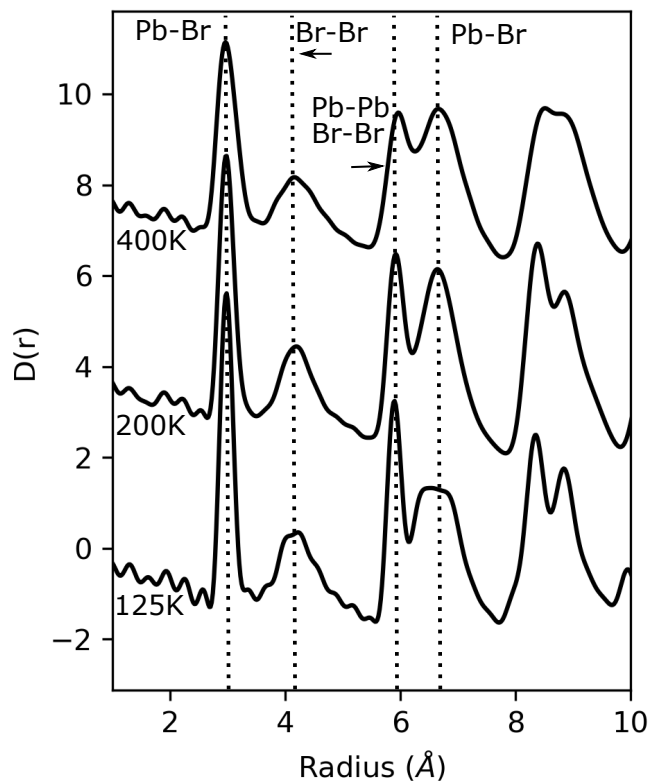


Figure 1. Pair distribution functions of $MAPbBr_3$ are shown in three different phases (orthorhombic, tetragonal and cubic, shown top to bottom). Each PDF is shown with a offset of 4 between them. Similar plots for $X = I$ and Cl are given in the SI.

(γ -butyrolactone) at room temperature. Then the obtained $MAPbI_3$ solution was heated to 110 °C for the crystal growth. Powder samples of $MAPbBr_3$ were prepared by the reaction of stoichiometric amounts of lead acetate and methylamine hydrobromide in hydrobromic acid. The excess acid was then evaporated to leave an orange colored product which was washed with diethyl ether. Powder samples of $MAPbCl_3$ were prepared out of a solution of methylamine hydrochloride and lead acetate dissolved in hydrochloric acid. An excess of an approximately 8-10 molar ratio of methylamine hydrochloride was required to obtain these phase pure samples. The resulting powder was washed with diethyl ether.

For $MAPbBr_3$, synchrotron radiation X-ray total scattering experiments were conducted at the synchrotron facility PETRA III (beamline P02.1³⁷) at DESY, Hamburg. A wavelength $\lambda = 0.2070 \text{ \AA}$ was used to collect data. Data were collected at temperatures of 125, 140, 147, 152 K and at intervals of 25 K from 175 to 450 K.

For $MAPbI_3$ and $MAPbCl_3$, Synchrotron radiation X-ray total scattering experiments were conducted at the synchrotron facility Diamond Light Source (beamline I15-1). A wavelength of $\lambda = 0.161669 \text{ \AA}$ was used to collect data. Data were collected at 20 K intervals over the temperature ranges 100 - 460 K ($MAPbCl_3$) and 100

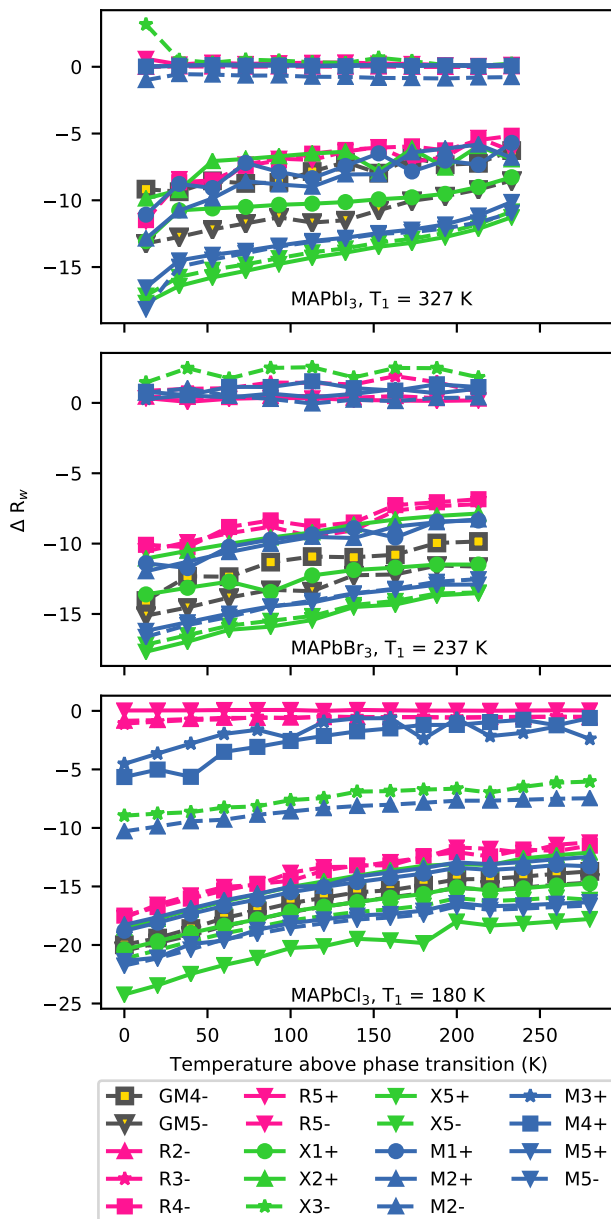


Figure 2. For each compound, the best individual fitting statistic is plotted for each irrep at each temperature. The R-factor is shown relative to the R-factor for the refinement with no symmetry adapted displacement modes active in the refinement, and the temperature shown is relative to the cubic phase transition as reported in the literature. The cubic transition temperature for each compound is indicated on the plot. The irreps are labelled as follows: colour denotes the k-point of the irrep, with blue referring to the M-point, green to X, pink to R and yellow to Γ ; marker shape denotes the irrep number, with a circle referring to 1, an upward-pointed triangle to 2, a star to 3, a square to 4 and a downward-pointed triangle to 5; linestyle denotes the parity of the irrep, with a solid line referring to a “+” irrep, and a dashed line referring to a “-” irrep.

- 560 K (MAPbI₃).

The obtained 2D images were masked and radially integrated using the DAWN³⁸ software. $G(r)$ and $D(r)$ functions were computed using GudrunX³⁹, using Q_{max} values of 21, 30 and 28 \AA^{-1} for MAPbBr₃, MAPbCl₃ and MAPbI₃ respectively. GudrunX was also used to perform background subtraction, sample absorption and fluorescence corrections.

Analysis of the pair distribution functions was carried out using the symmetry-adapted PDF analysis (SAPA) method described in ref. 32. For each sample, a $2 \times 2 \times 2$ $P1$ supercell of the $Pm\bar{3}m$ aristotype PbX_3 with Pb at (0.5, 0.5, 0.5) and X at (0.5, 0.5, 0) was generated and parameterised in terms of symmetry adapted displacements using the ISODISTORT software⁴⁰. The generated mode listings were output in .cif format and then converted to the .inp format of the TOPAS Academic software v6 using the Jedit macros⁴¹. In total, there were 96 modes which transformed according to one of 19 irreducible representations. These supercells were generated without the organic A-site cation included, since the contribution of pairs involving the organic components of the structure will have a negligible contribution to the overall PDF due to their comparatively weak scattering power for X-rays. This lack of sensitivity of X-ray total scattering to the organic elements of hybrid perovskites can be seen by comparing recent publications by Malavasi *et al*^{42–44}. For each irreducible representation (irrep) at each temperature, refinements of the corresponding modes were started from random starting mode amplitudes. This was repeated 500 times. For all samples, the refinements were carried out with a fitting range of 1.7 to 20 \AA . Refinements were also tested using a fitting range with a maximum of 10 \AA and found to be broadly similar.

The DFT calculations were performed using the Vienna Ab Initio Simulation Package (VASP)^{45–48}, version 5.4.4. We employed the optB86b-vdW exchange correlation potential⁴⁹ which includes VdW corrections previously found to suit hybrid perovskites²⁴. Projector augmented-wave (PAW) pseudopotentials^{46,50} were utilised, as supplied within the VASP package. A plane wave basis set with a 1100 eV energy cutoff and a $4 \times 4 \times 4$ Monkhorst-Pack k-point mesh with respect to the parent cubic primitive cell (scaled accordingly for other supercells) were found suitable. The energy landscape of the various modes in the hybrid system were studied by fixing the halide framework while allowing for Pb and MA to relax until the forces were less than 5 meV/ \AA . Results were compared with FrPbBr₃, which we used as a hypothetical inorganic analogue to the hybrid perovskite, since Fr best matches the ionic radii of MA²⁴.

III. RESULTS AND DISCUSSION

A key aspect of the local structure of the MAPbX₃ (X = I, Br, Cl) family of hybrid perovskites is that the first four peaks of the inorganic component of the PDF do

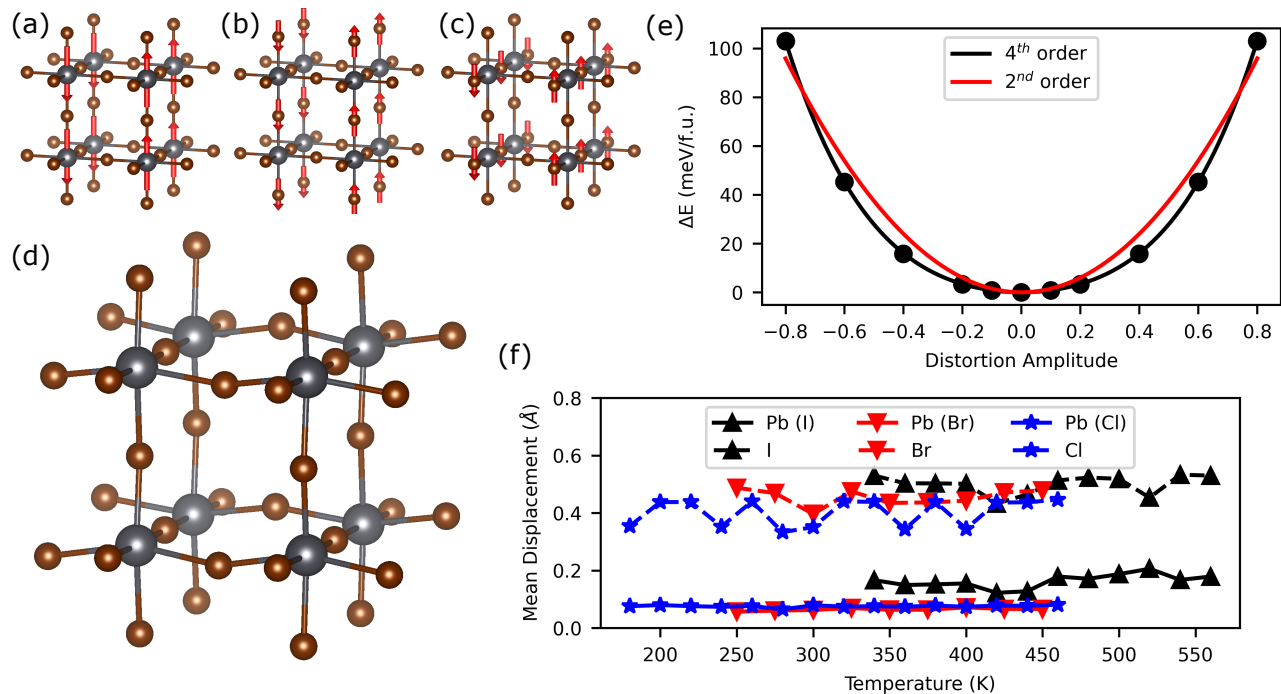


Figure 3. (a-c) A breakdown of the atomic basis that spans the X_5^+ irrep. Shown in (d) is the structure resulting from a refinement of the $Pnma$ order parameter direction of the X_5^+ irrep. (e) Mode energies with varying distortion mode amplitude for the $Pnma$ order parameter direction of FrPbBr_3 . Harmonic (2nd order) and anharmonic (4th order) fits to the potential well are shown. (f) Mean displacement values for the general X_5^+ order parameter direction.

not change much beyond that expected for simply changing the temperature, i.e a change in peak width corresponding to a change in thermal energy, and a change in peak position corresponding to thermal expansion. For MAPbBr_3 (Fig. 1) and MAPbCl_3 , the peaks stay the same from the low temperature orthorhombic phase into the high temperature cubic phase^{42–44}. For MAPbI_3 , there is a slight change upon the transition between the tetragonal and orthorhombic phases, but the peaks from the tetragonal phase persist in the cubic phase⁵¹ (see SI). This has been taken to imply that the cubic phase consists of local symmetry-broken domains and there has been recent work to support this hypothesis⁵¹. This would suggest that the distortions most responsible for the local structure should be the rigid-unit modes (RUMs) that drive these phase transitions.

To gain a more robust understanding of the local structure of MAPbX_3 ($X = \text{I}, \text{Br}, \text{Cl}$), we perform a symmetry-adapted PDF analysis (SAPA)^{34,35} to elucidate the character of the dominant lattice dynamics associated with the inorganic cage. We note that we are insensitive to MA orientation and displacement modes in the present X-ray PDF study, and so no attempt is made to model these against the experimental data. The symmetry-adapted displacements which show the most improvement in the R_w for the models against the PDFs for all compounds and all temperatures are those which transform according to irreps that permit a scissoring motion

of the X anions, *i.e.*, the Br–Pb–Br bond angles are distorted away from 90° but the Pb–Br bond lengths remain undistorted. This result of the SAPA analysis does not imply that the RUMs are high energy modes, it simply means that the majority of the motion of the halide anions arise from these scissoring modes. This is supported by competitive two-phase refinements of the PDFs, in which we allow the X_5^+ displacements to refine in one phase and the displacements for one of the RUMs (R_5^- or M_2^+) in the other. These refinements show a preference for scissoring modes compared to the RUMs for all 3 samples, as evident from the refined scale factors of the two phases which show an approximate scissoring:rotation ratio of 2.3:1 (see SI for more details). For context, this ratio is approximately 4:1 in ScF_3 , which is isostructural to the inorganic framework of MAPbX_3 . The lower ratio compared to ScF_3 reflects a lower flexibility due to the presence of an A -site cation, which can interact with the inorganic framework *via* hydrogen bonding²³. However, it is clear from our results that the majority of the halide anion motion still arises from scissoring-type deformations of the octahedra.

The above results are in line with a recent reverse Monte Carlo (RMC) analysis of neutron PDFs of MAPbI_3 ⁵² between 10 and 400 K. This study demonstrates that a bending of the Pb–I–Pb bond angle dominates the local distortions of the PbI_6 octahedra. Our results show that the four best fitting modes all have

scissoring character, of which it is the X_5^+ (Fig 3 (c&d)) that performs best across all three compositions and temperatures. This could be due to the fact that there are more parameters for the X_5^+ irrep than the other three (18 modes transform as the X_5^+ irrep, compared to 12 for M_5^- and 6 for X_5^- and M_5^+), but the improvement could arise from the anti-polar Pb displacements that enter into the irrep X_5^+ , although this is unlikely since they only have a small contribution to the overall displacements. The three distortions that span this irrep are shown in Fig 3. We find the amplitudes of these scissoring modes to be quite large; refinements of X_5^+ and X_5^- in the tetragonal phase of MAPbBr₃ resulted in supercell-normalised mode amplitudes of ≈ 1.35 Å. This is close in magnitude to the equivalent amplitude of the R_5^- distortion (≈ 1.65 Å) which is frozen into the structure in the tetragonal phase.

Given how large the local deviations are from the average structure, it is reasonable to assume they will have a substantial effect on the band structure. We used DFT calculations to investigate the impact that the scissoring modes could have on the electronic band structure of the hybrid perovskites. We chose to analyse MAPbBr₃, since it is cubic at room temperature where experimental band gap values have been reported, and to focus on the two X point modes that do the best job at describing the deviations away from local cubic symmetry, as evident in the PDF data. For a completely unrestrained order parameter direction transforming as X_5^+ , there are a rather large number of degrees of freedom (18 in total), so, to make our results more robust, and to facilitate a direct comparison to X_5^- , we take results from refinements using higher symmetry OPDs with no more than 5 parameters. We use structures from refinements against our data with X_5^+ OPDs with $Pnma$ and $Cmcm$ symmetry ($(0, a; b, 0; 0, c)$ and $(0, a; b, b; a, 0)$ respectively) and the X_5^- OPD with $C2/c$ symmetry ($(a, b; c, -c; -b, -a)$) as input to our band structure calculations. For the two X_5^+ OPDs, only Br anion displacements were refined when generating the CIFs for the band structure calculations, although by symmetry, Pb displacements also enter into the irrep. For X_5^- , Pb displacements are forbidden by symmetry. We also sampled points of different overall distortion amplitude along the X_5^+ OPD with $Pnma$ symmetry and calculated the energy. These energy calculations were performed for the FrPbBr₃ structures used to calculate the band structure.

In the undistorted structure, the calculated band gap was 1.717 eV, which is slightly higher than other calculated band gaps for cubic MAPbBr₃ (1.64 eV⁵³) at the same level of theory, and is direct. Previous work has shown that substitution of Fr for MA opens up the band gap slightly in orthorhombic MAPbI₃²⁴. For each distortion, the band gap opens up significantly to values of 2.025, 2.138 and 2.162 eV for the $C2/c$, $Cmcm$ and $Pnma$ distortions with an amplitude of $0.8\times$ the maximum amplitude refined from PDF data for the X_5^+ distortions and $1.1\times$ the maximum amplitude for X_5^- , re-

spectively, and remains direct. These relative amplitudes were chosen so all 3 distortions were at similar mode amplitudes. These values are closer to the experimentally determined band gaps for MAPbBr₃ of ≈ 2.3 eV at room temperature⁵⁴, although this is likely due to a cancellation of errors. The distortions result in a reduced orbital overlap between Pb and Br p-orbitals, leading to a lower band curvature and therefore an increased effective mass in the distorted band structures (Fig 4 and SI). The mobility of polarons is inversely proportional to the electron band effective mass⁵⁵, and this increased effective mass in the distorted structures may explain the discrepancy between experimental and calculated values⁵⁶.

Spin-orbit coupling (SOC) interactions, which play a large role in systems involving Pb, have not been accounted for. Consequently, the exact shape of the electron bands and size of the band gap won't be accurate, since inclusion of SOC has been shown to lead to unconventional dispersion relations⁵⁷. The effects from SOC on band gap size in halide perovskites tend to be canceled out by full treatment of electron Coulomb interactions beyond DFT^{58,59}. Therefore, the trends we detect due to the different distortion modes will remain the same. In the two X_5^+ distortions, the degeneracy of the bands at the conduction band minimum (CBM) at the Γ point are broken, leading to fewer available states at the CBM. Contrastingly, the X_5^+ $Pnma$ distortion appears to have the largest DOS at the valence band maximum due to the reduced bandwidth. Fluctuations in the band gap of hybrid perovskites due to their highly dynamic structure has been previously predicted³², and is expected to assist the initial stages of charge separation. In addition, an increase of the band gap coinciding with a transverse displacement of I ions in MAPbI₃ due to an external strain field has been reported³³.

Our refinements against the PDF data show that all three modes have a large amplitude, with supercell-normalised mode amplitudes of 1.84, 1.82 and 1.36 Å for OPDs with $Pnma$, $Cmcm$ and $C2/c$ symmetries, respectively. These mode amplitudes correspond to maximum Br displacements of 0.486, 0.410 and 0.350 Å. Note that the refined distortions correspond to a time-averaged view of the structure, so these maximum Br displacements are a factor of $\sqrt{2}\times$ greater, in the harmonic approximation, than those found in the refined structures. As a consequence of their large amplitudes, the distortions would be expected to be anharmonic in nature, which is supported by the potential energy well we calculate for the X_5^+ $(0, a; b, 0; 0, c)$ OPD in FrPbBr₃ (Fig 3 (f)), which has a significant quartic component when fit with a 4th order polynomial fit ($\Delta E = 127x^4 + 79.7x^2$, where x is the distortion mode amplitude relative to its maximum value at 400 K). This breakdown in the harmonic approximation would then allow the scissoring modes of the inorganic framework to couple directly to the anharmonic modes that correspond to the organic cation dynamics^{60,61}. Despite the presence of an A-site in these materials, the amplitude of these scissoring modes

are greater than those in ScF_3 , suggesting the MA cations move to accommodate the large-amplitude modes. The implication of this, then, is that the band gap opening we detect as a response to the scissoring modes is likely influenced by the dynamics of the MA cations, although our refinements are only sensitive to the inorganic framework.

To investigate the above hypothesis, we consider the X_5^+ OPD with $Pnma$ symmetry. This breaks the equivalence of the $\langle 100 \rangle$ directions and leads to two distinct A-site symmetries (see SI). Therefore, if the inorganic and organic dynamics are coupled together, we would expect to see the MA cations located at different points of the unit cell to respond differently to the distortion mode, to reflect the different local environments they would experience. To test this, we relaxed the MA cations from an initial anti-polar configuration with the C-N bonds aligned with the $[100]$ direction, in a structure with a $0.8 \times X_5^+$ ($0, a; b, 0; 0, c$) distortion (relative to the maximum amplitude at 400 K) frozen in. The MA cations showed significant reorientation, with the “edge” ($(0.5, 0, 0)$ and equivalents) and “corner” ($(0, 0, 0)$) cations rotating to include significant components along c . There is a split amongst the “face” cations, with two (at $(0.5, 0.5, 0)$ and $(0, 0.5, 0.5)$) rotating to include smaller components along the b - and c -axes. The remaining “face” cation and the cation located at the centre of the supercell both rotate to include a significant component along c and a smaller component along b . In all, there are 5 distinct C-N bond alignments, which may reflect the 5 distinct Br sites. In addition, all cations show a slight displacement from the high-symmetry-unique positions. Full details can be found in the SI. This demonstrates that the MA cations can rotate to accommodate the distortions of the inorganic framework, indicating that the dynamics of the two components of the structure may be linked. However, it is important to note that our calculations are effectively performed at 0 K, where the ground state is the fully ordered orthorhombic phase. It is quite possible that the configurational entropy associated with the MA orderings may effectively act to decouple these dynamics at higher temperatures in the cubic phase. Indeed, there is evidence to suggest the organic and inorganic dynamics are decoupled in MAPbCl_3 ¹³. Additionally, a similar computational result in CsPbBr_3 showing coupling between large amplitude distortions of the Br ions and head-to-head Cs motion⁶² suggest this feature may not be exclusive to hybrid inorganic systems. We have also shown that acoustic phonon lifetimes for the all-inorganic CsPbBr_3 are very similar to those in MAPbCl_3 ⁶³, further supporting the idea that at high temperatures the MA rotational modes may have little effect on the lattice phonon modes.

There has been recent literature support for the idea that cubic halide perovskites, rather than being treated as a single repeating unit, should be thought of as a network of polymorphs showing different symmetry-lowering deformations of the average structure, such as varying degrees of octahedral tilting or differing amplitudes of

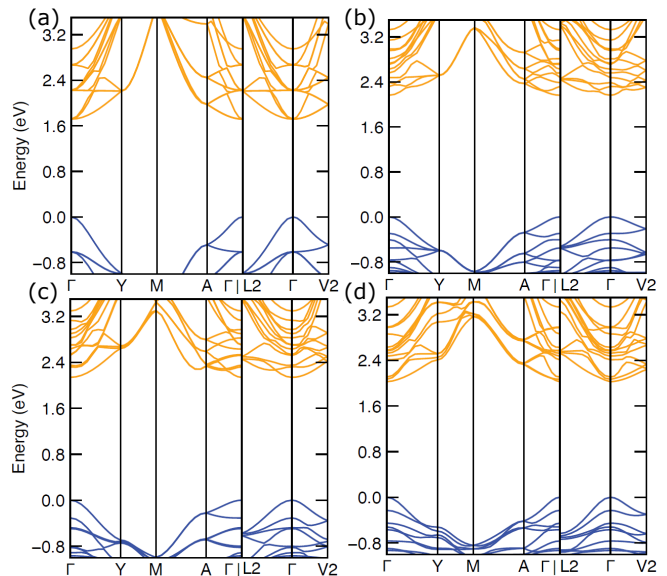


Figure 4. The calculated electronic band structure of FrPbBr_3 for the undistorted structure (a), the $Pnma$ and Cmc order parameter directions of the X_5^+ irrep (b and c, respectively) and the $C2/c$ order parameter direction of the X_5^- irrep (d). These figures were created using sumo⁶⁵

B-site displacement⁶⁴. Our work is broadly consistent with this picture. The stereochemical behaviour of the Pb cation, in conjunction with the coupling between organic cation and inorganic framework dynamics, is likely to have a large impact on the possible polymorphs the material exhibits within this hypothesis of the nature of the structure of halide perovskites.

In summary, we have shown that large scissoring modes of the halide ions describe the dominant deviations from the average structure in the cubic phases of the hybrid perovskites. These modes have a similar amplitude to those of the static RUMs below the phase transition temperature. These distortions have the effect of opening up the band gap of the electronic structure. In addition, we have shown that the organic cations can move to accommodate the distortions of the inorganic framework, suggesting the dynamics of the two components could be inherently linked, and that the inorganic lattice is likely to be significantly distorted from the average at a local level. These dynamic structures should be accounted for in simulations performed on the hybrid perovskites, since they can have a significant effect on the calculated properties.

The PDF data used in this study are available as a supporting dataset.

ACKNOWLEDGEMENTS

T.A.B thanks EPSRC for a PhD studentship through the EPSRC Centre for Doctoral Training in Molecular Analytical Science, grant number EP/L015307/1. M.S.S

acknowledges the Royal Society for a University Research Fellowship (UF160265). N.C.B acknowledges computational resources from the Hamilton HPC Service of Durham University and the UK Materials and Molecular Modelling Hub (partially funded by the EPSRC project EP/P020194/1). We acknowledge DESY (Hamburg, Germany), a member of the Helmholtz Association

HGF, for the provision of experimental facilities. Parts of this research were carried out at PETRA III. We also thank Diamond Light Source for providing experiment time on beamline I15-1 under proposal number CY21611. Samples were characterised via Block Allocation Group Award (EE18786) at the high resolution powder diffractometer I11, Diamond Light Source.

-
- * m.senn@warwick.ac.uk
- ¹ Akihiro Kojima, Kenjiro Teshima, Yasuo Shirai, and Tsutomu Miyasaka, "Organometal Halide Perovskites as Visible-Light Sensitizers for Photovoltaic Cells," *J. Am. Chem. Soc.* **131**, 6050–6051 (2009).
 - ² Martin A. Green, Anita Ho-Baillie, and Henry J. Snaith, "The emergence of perovskite solar cells," *Nat. Photonics* **8**, 506–514 (2014).
 - ³ Olga Malinkiewicz, Aswani Yella, Yong Hui Lee, Guillermo Mínguez Espallargas, Michael Graetzel, Mohammad K. Nazeeruddin, and Henk J. Bolink, "Perovskite solar cells employing organic charge-transport layers," *Nat. Photonics* **8**, 128–132 (2014).
 - ⁴ Giorgio Schileo and Giulia Grancini, "Halide perovskites: current issues and new strategies to push material and device stability," *J. Phys.: Energy* **2**, 021005 (2020).
 - ⁵ Christian Wehrenfennig, Giles E. Eperon, Michael B. Johnston, Henry J. Snaith, and Laura M. Herz, "High charge carrier mobilities and lifetimes in organolead trihalide perovskites," *Adv. Mater.* **26**, 1584–1589 (2014).
 - ⁶ Daming Zhao, Jonathan M. Skelton, Hongwei Hu, Chan La-o vorakiat, Jian-Xin Zhu, Rudolph A. Marcus, Maria-Elisabeth Michel-Beyerle, Yeng Ming Lam, Aron Walsh, and Elbert E. M. Chia, "Low-frequency optical phonon modes and carrier mobility in the halide perovskite CH₃NH₃PbBr₃ using terahertz time-domain spectroscopy," *Appl. Phys. Lett.* **111**, 201903 (2017).
 - ⁷ Guichuan Xing, Nripan Mathews, Shuangyong Sun, Swee Sien Lim, Yeng Ming Lam, Michael Grätzel, Subodh Mhaisalkar, and Tze Chien Sum, "Long-range balanced electron- and hole-transport lengths in organic-inorganic CH₃NH₃PbI₃," *Science* **342**, 344–347 (2013).
 - ⁸ Shuangyong Sun, Teddy Salim, Nripan Mathews, Martial Duchamp, Chris Boothroyd, Guichuan Xing, Tze Chien Sum, and Yeng Ming Lam, "The origin of high efficiency in low-temperature solution-processable bilayer organometal halide hybrid solar cells," *Energy Environ. Sci.* **7**, 399–407 (2014).
 - ⁹ Yu-Che Hsiao, Ting Wu, Mingxing Li, Qing Liu, Wei Qin, and Bin Hu, "Fundamental physics behind high-efficiency organo-metal halide perovskite solar cells," *J. Mater. Chem. A* **3**, 15372–15385 (2015).
 - ¹⁰ Aurélien M. A. Leguy, Alejandro R. Goni, Jarvist M. Frost, Jonathan Skelton, Federico Brivio, Xabier Rodríguez-Martínez, Oliver J. Weber, Anuradha Pallipurath, M. Isabel Alonso, Mariano Campoy-Quiles, Mark T. Weller, Jenny Nelson, Aron Walsh, and Piers R. F. Barnes, "Dynamic disorder, phonon lifetimes, and the assignment of modes to the vibrational spectra of methylammonium lead halide perovskites," *Phys. Chem. Chem. Phys.* **18**, 27051–27066 (2016).
 - ¹¹ Antoine Létoublon, Serge Paofai, Benoît Rufflé, Philippe Bourges, Bernard Hehlen, Thierry Michel, Claude Ecolivet, Olivier Durand, Stéphane Cordier, Claudine Katan, and Jacky Even, "Elastic Constants, Optical Phonons, and Molecular Relaxations in the High Temperature Plastic Phase of the CH₃NH₃PbBr₃ Hybrid Perovskite," *J. Phys. Chem. Lett.* **7**, 3776–3784 (2016).
 - ¹² K. L. Brown, S. F. Parker, I. Robles García, S. Mukhopadhyay, V. García Sakai, and C. Stock, "Molecular orientational melting within a lead-halide octahedron framework: The order-disorder transition in CH₃NH₃PbBr₃," *Phys. Rev. B* **96**, 174111 (2017).
 - ¹³ M. Songvilay, Zitian Wang, V. Garcia Sakai, T. Guidi, M. Bari, Z. G. Ye, Guangyong Xu, K. L. Brown, P. M. Gehring, and C. Stock, "Decoupled molecular and inorganic framework dynamics in CH₃NH₃PbCl₃," *Phys. Rev. Mater.* **3**, 125406 (2019).
 - ¹⁴ Andrea Pisoni, Jaćim Jaćimović, Osor S. Barišić, Massimo Spina, Richard Gaál, László Forró, and Endre Horváth, "Ultra-low thermal conductivity in organic-inorganic hybrid perovskite CH₃NH₃PbI₃," *J. Phys. Chem. Lett.* **5**, 2488–2492 (2014).
 - ¹⁵ M Nadim Ferdous Hoque, Mengjin Yang, Zhen Li, Nazifah Islam, Xuan Pan, Kai Zhu, and Zhaoyang Fan, "Polarization and Dielectric Study of Methylammonium Lead Iodide Thin Film to Reveal its Nonferroelectric Nature under Solar Cell Operating Conditions," *ACS Energy Lett.* **1**, 142–149 (2016).
 - ¹⁶ Joanna Jankowska and Oleg V. Prezhdo, "Ferroelectric Alignment of Organic Cations Inhibits Nonradiative Electron-Hole Recombination in Hybrid Perovskites: Ab Initio Nonadiabatic Molecular Dynamics," *J. Phys. Chem. Lett.* **8**, 812–818 (2017).
 - ¹⁷ J. Breternitz, F. Lehmann, S. A. Barnett, H. Nowell, and S. Schorr, "Role of the Iodide–Methylammonium Interaction in the Ferroelectricity of CH₃NH₃PbI₃," *Angew. Chem. Int. Ed.* **59**, 424–428 (2020).
 - ¹⁸ A. Poglitsch and D. Weber, "Dynamic disorder in methylammoniumtrihalogenoplumbates (II) observed by millimeter-wave spectroscopy," *J. Chem. Phys.* **87**, 6373–6378 (1987).
 - ¹⁹ Yinsheng Guo, Omer Yaffe, Daniel W. Paley, Alexander N. Beecher, Trevor D. Hull, Guilherme Szpak, Jonathan S. Owen, Louis E. Brus, and Marcos A. Pimenta, "Interplay between organic cations and inorganic framework and incommensurability in hybrid lead-halide perovskite CH₃NH₃PbBr₃," *Phys. Rev. Mater.* **1**, 042401 (2017).
 - ²⁰ Tianran Chen, Benjamin J. Foley, Bahar Ipek, Madhusudan Tyagi, John R. D. Copley, Craig M. Brown, Joshua J. Choi, and Seung-Hun Lee, "Rotational dynamics of organic cations in the CH₃NH₃PbI₃ perovskite," *Phys. Chem. Chem. Phys.* **17**, 31278–31286 (2015).

- ²¹ Aurelien M.A. Leguy, Jarvist Moore Frost, Andrew P. McMahon, Victoria Garcia Sakai, W. Kochelmann, Chun-hung Law, Xiaoe Li, Fabrizia Foglia, Aron Walsh, Brian C. O'Regan, Jenny Nelson, João T. Cabral, and Piers R.F. Barnes, "The dynamics of methylammonium ions in hybrid organic-inorganic perovskite solar cells," *Nat. Commun.* **6**, 7124 (2015).
- ²² Mark T. Weller, Oliver J. Weber, Paul F. Henry, Antonietta M. Di Pumpo, and Thomas C. Hansen, "Complete structure and cation orientation in the perovskite photovoltaic methylammonium lead iodide between 100 and 352 K," *Chem. Commun.* **51**, 4180–4183 (2015).
- ²³ Jung Hoon Lee, Nicholas C. Bristowe, Paul D. Bristowe, and Anthony K. Cheetham, "Role of hydrogen-bonding and its interplay with octahedral tilting in CH₃NH₃PbI₃," *Chem. Commun.* **51**, 6434–6437 (2015).
- ²⁴ Jung Hoon Lee, Nicholas C. Bristowe, June Ho Lee, Sung Hoon Lee, Paul D. Bristowe, Anthony K. Cheetham, and Hyun Myung Jang, "Resolving the Physical Origin of Octahedral Tilting in Halide Perovskites," *Chem. Mater.* **28**, 4259–4266 (2016).
- ²⁵ Nicholas Aristidou, Christopher Eames, Irene Sanchez-Molina, Xiangnan Bu, Jan Kosco, M. Saiful Islam, and Saif A. Haque, "Fast oxygen diffusion and iodide defects mediate oxygen-induced degradation of perovskite solar cells," *Nat. Commun.* **8**, 15218 (2017).
- ²⁶ Dibyajyoti Ghosh, Philip Walsh Atkins, M. Saiful Islam, Alison B. Walker, and Christopher Eames, "Good Vibrations: Locking of Octahedral Tilting in Mixed-Cation Iodide Perovskites for Solar Cells," *ACS Energy Lett.* **2**, 2424–2429 (2017).
- ²⁷ Christopher Eames, Jarvist M. Frost, Piers R.F. Barnes, Brian C. O'Regan, Aron Walsh, and M. Saiful Islam, "Ionic transport in hybrid lead iodide perovskite solar cells," *Nat. Commun.* **6**, 7497 (2015).
- ²⁸ Ana L. Montero-Alejo, E. Menéndez-Proupin, D. Hidalgo-Rojas, P. Palacios, P. Wahnón, and J. C. Conesa, "Modeling of Thermal Effect on the Electronic Properties of Photovoltaic Perovskite CH₃NH₃PbI₃: The Case of Tetragonal Phase," *J. Phys. Chem. C* **120**, 7976–7986 (2016).
- ²⁹ Marcelo A. Carignano, Ali Kachmar, and Jürg Hutter, "Thermal Effects on CH₃NH₃PbI₃ Perovskite from Ab Initio Molecular Dynamics Simulations," *J. Phys. Chem. C* **119**, 8991–8997 (2015).
- ³⁰ A. Mattoni, A. Filippetti, M. I. Saba, and P. Delugas, "Methylammonium Rotational Dynamics in Lead Halide Perovskite by Classical Molecular Dynamics: The Role of Temperature," *J. Phys. Chem. C* **119**, 17421–17428 (2015).
- ³¹ Claudio Quarti, Edoardo Mosconi, and Filippo De Angelis, "Interplay of orientational order and electronic structure in methylammonium lead iodide: Implications for solar cell operation," *Chem. Mater.* **26**, 6557–6569 (2014).
- ³² Claudio Quarti, Edoardo Mosconi, and Filippo De Angelis, "Structural and electronic properties of organo-halide hybrid perovskites from ab initio molecular dynamics," *Phys. Chem. Chem. Phys.* **17**, 9394–9409 (2015).
- ³³ Le Zhang, Wei Geng, Chuan Jia Tong, Xueguang Chen, Tengfei Cao, and Mingyang Chen, "Strain induced electronic structure variation in methyl-ammonium lead iodide perovskite," *Sci. Rep.* **8**, 7760 (2018).
- ³⁴ M. S. Senn, D. A. Keen, T. C.A. Lucas, J. A. Hriljac, and A. L. Goodwin, "Emergence of Long-Range Order in BaTiO₃ from Local Symmetry-Breaking Distortions," *Phys. Rev. Lett.* **116**, 207602 (2016).
- ³⁵ T. A. Bird, J. Woodland-Scott, L. Hu, M. T. Wharmby, J. Chen, A. L. Goodwin, and M. S. Senn, "Anharmonicity and scissoring modes in the negative thermal expansion materials ScF₃ and CaZrF₆," *Phys. Rev. B* **101**, 064306 (2020).
- ³⁶ Makhstud I. Saidaminov, Ahmed L. Abdelhady, Banavoth Murali, Erkki Alarousu, Victor M. Burlakov, Wei Peng, Ibrahim Dursun, Lingfei Wang, Yao He, Giacomo MacUlan, Alain Goriely, Tom Wu, Omar F. Mohammed, and Osman M. Bakr, "High-quality bulk hybrid perovskite single crystals within minutes by inverse temperature crystallization," *Nat. Commun.* **6**, 7586 (2015).
- ³⁷ Ann-Christin Dippel, Hanns-Peter Liermann, Jan Torben Delitz, Peter Walter, Horst Schulte-Schrepping, Oliver H. Seeck, and Hermann Franz, "Beamline P02.1 at PETRA III for high-resolution and high-energy powder diffraction," *J. Synchrotron Radiat.* **22**, 675–687 (2015).
- ³⁸ Mark Basham, Jacob Filik, Michael T. Wharmby, Peter C.Y. Chang, Baha El Kassaby, Matthew Gerring, Jun Aishima, Karl Levik, Bill C.A. Pulford, Irakli Sikharulidze, Duncan Sneddon, Matthew Webber, Sarnjeet S. Dhesi, Francesco Maccherozzi, Olof Svensson, Sandor Brockhauser, Gabor Náráy, and Alun W. Ashton, "Data Analysis Workbench (DAWN)," *J. Synchrotron Radiat.* **22**, 853–858 (2015).
- ³⁹ S. E. McLain, D. T. Bowron, A. C. Hannon, and A. K. Soper, "GUDRUN, a computer program developed for analysis of neutron diffraction data, Chilton: ISIS Facility, Rutherford Appleton Laboratory," (2012).
- ⁴⁰ Branton J Campbell, Harold T Stokes, David E Tanner, and Dorian M Hatch, "ISODISPLACE: A web-based tool for exploring structural distortions," *J. Appl. Crystallogr.* **39**, 607–614 (2006).
- ⁴¹ John S.O. Evans, "Advanced input files & parametric quantitative analysis using topas," *Mater. Sci. Forum* **651**, 1–9 (2010).
- ⁴² Katharine Page, Joan E. Siewenie, Paolo Quadrelli, and Lorenzo Malavasi, "Short-Range Order of Methylammonium and Persistence of Distortion at the Local Scale in MAPbBr₃Hybrid Perovskite," *Angew. Chem. Int. Ed.* **55**, 14320–14324 (2016).
- ⁴³ Andrea Bernasconi and Lorenzo Malavasi, "Direct evidence of permanent octahedra distortion in MAPbBr₃ hybrid perovskite," *ACS Energy Lett.* **2**, 863–868 (2017).
- ⁴⁴ Andrea Bernasconi, Katharine Page, Zhenbang Dai, Liang Z. Tan, Andrew M. Rappe, and Lorenzo Malavasi, "Ubiquitous Short-Range Distortion of Hybrid Perovskites and Hydrogen-Bonding Role: The MAPbCl₃ Case," *J. Phys. Chem. C* **122**, 28265–28272 (2018).
- ⁴⁵ G. Kresse and J. Hafner, "Ab initio molecular-dynamics simulation of the liquid-metalamorphous- semiconductor transition in germanium," *Phys. Rev. B* **49**, 14251–14269 (1994).
- ⁴⁶ G. Kresse and J. Furthmüller, "Efficient iterative schemes for ab initio total-energy calculations using a plane-wave basis set," *Phys. Rev. B* **54**, 11169 – 11186 (1996).
- ⁴⁷ G. Kresse and J. Furthmüller, "Efficiency of ab-initio total energy calculations for metals and semiconductors using a plane-wave basis set," *Comput. Mater. Sci.* **6**, 15–50 (1996).
- ⁴⁸ G. Kresse and J. Hafner, "Ab initio molecular dynamics for liquid metals," *J. Non-Cryst. Solids* **47**, 558–561 (1993).
- ⁴⁹ Jiří Klimes, David R. Bowler, and Angelos Michaelides, "Van der Waals density functionals applied to solids,"

- Phys. Rev. B **83**, 195131 (2011).
- ⁵⁰ P E Blochl, “Projector augmented-wave method,” Phys. Rev. B **50**, 17953–17979 (1994).
- ⁵¹ Alexander N. Beecher, Octavi E. Semonin, Jonathan M. Skelton, Jarvist M. Frost, Maxwell W. Terban, Haowei Zhai, Ahmet Alatas, Jonathan S. Owen, Aron Walsh, and Simon J.L. Billinge, “Direct Observation of Dynamic Symmetry Breaking above Room Temperature in Methylammonium Lead Iodide Perovskite,” ACS Energy Lett. **1**, 880–887 (2016).
- ⁵² Jiaxun Liu, *Local structure of lead halide perovskites for photovoltaic applications*, Doctor of philosophy, Queen Mary, University of London (2017).
- ⁵³ Edoardo Mosconi, Paolo Umari, and Filippo De Angelis, “Electronic and optical properties of MAPbX₃ perovskites (X = I, Br, Cl): A unified DFT and GW theoretical analysis,” Phys. Chem. Chem. Phys. **18**, 27158–27164 (2016).
- ⁵⁴ G. C. Papavassiliou and I. B. Koutselas, “Structural, optical and related properties of some natural three- and lower-dimensional semiconductor systems,” Synth. Met. **71**, 1713–1714 (1995).
- ⁵⁵ Jarvist Moore Frost, “Calculating polaron mobility in halide perovskites,” Phys. Rev. B **96**, 195202 (2017).
- ⁵⁶ Mischa Bonn, Kiyoshi Miyata, Euan Hendry, and X. Y. Zhu, “Role of Dielectric Drag in Polaron Mobility in Lead Halide Perovskites,” ACS Energy Lett. **2**, 2555–2562 (2017).
- ⁵⁷ Federico Brivio, Keith T. Butler, Aron Walsh, and Mark Van Schilfgaarde, “Relativistic quasiparticle self-consistent electronic structure of hybrid halide perovskite photovoltaic absorbers,” Phys. Rev. B **89**, 155204 (2014).
- ⁵⁸ Jacky Even, Laurent Pedesseau, Jean Marc Jancu, and Claudine Katan, “Importance of spin-orbit coupling in hybrid organic/inorganic perovskites for photovoltaic applications,” J. Phys. Chem. Lett. **4**, 2999–3005 (2013).
- ⁵⁹ Paolo Umari, Edoardo Mosconi, and Filippo De Angelis, “Relativistic GW calculations on CH₃NH₃PbI₃ and CH₃NH₃SnI₃ Perovskites for Solar Cell Applications,” Sci. Rep. **4**, 4467 (2014).
- ⁶⁰ Bing Li, Yukinobu Kawakita, Yucheng Liu, Mingchao Wang, Masato Matsuura, Kaoru Shibata, Seiko Ohira-Kawamura, Takeshi Yamada, Shangchao Lin, Kenji Nakajima, and Shengzhong Frank Liu, “Polar rotor scattering as atomic-level origin of low mobility and thermal conductivity of perovskite CH₃NH₃PbI₃,” Nat. Commun. **8**, 16086 (2017).
- ⁶¹ Tufan Ghosh, Sigalit Aharon, Lioz Etgar, and Sanford Ruhman, “Free Carrier Emergence and Onset of Electron-Phonon Coupling in Methylammonium Lead Halide Perovskite Films,” J. Am. Chem. Soc. **139**, 18262–18270 (2017).
- ⁶² Omer Yaffe, Yinsheng Guo, Liang Z. Tan, David A. Egger, Trevor Hull, Constantinos C. Stoumpos, Fan Zheng, Tony F. Heinz, Leeor Kronik, Mercouri G. Kanatzidis, Jonathan S. Owen, Andrew M. Rappe, Marcos A. Pimenta, and Louis E. Brus, “Local Polar Fluctuations in Lead Halide Perovskite Crystals,” Phys. Rev. Lett. **118**, 136001 (2017).
- ⁶³ M. Songvilay, N. Giles-Donovan, M. Bari, Z. G. Ye, J. L. Minns, M. A. Green, Guangyong Xu, P. M. Gehring, K. Schmalzl, W. D. Ratcliff, C. M. Brown, D. Chernyshov, W. Van Beek, S. Cochran, and C. Stock, “Common acoustic phonon lifetimes in inorganic and hybrid lead halide perovskites,” Phys. Rev. Mater. **3**, 093602 (2019).
- ⁶⁴ Xin Gang Zhao, Gustavo M. Dalpian, Zhi Wang, and Alex Zunger, “Polymorphous nature of cubic halide perovskites,” Phys. Rev. B **101**, 155137 (2020).
- ⁶⁵ Alex M. Ganose, Adam J. Jackson, and David O. Scanlon, “sumo: Command-line tools for plotting and analysis of periodic ab initio calculations,” J. Open Source Softw. **3**, 717 (2018).